Journal of Solid Mechanics Vol. 1, No. 3 (2009) pp. 233-244

Photoelastic Determination of Mixed Mode Stress Intensity Factors

V.K. Singh*, P.C. Gope

Department of Mechanical Engineering, College of Technology, G.B. Pant University of Agriculture & Technology, Pantnagar 263145, India

Received 17 November 2009; accepted 29 November 2009

ABSTRACT

A two dimensional finite model with inclined crack at different crack angles are being analyzed in mixed mode condition using photo elasticity method for the determination of Stress Intensity Factors. The well-known Sih's equation and three points deterministic approach is used for the determination of stress intensity factors. The effects of biaxial load factor, crack angle, size factors were studied and a regression model was developed for geometry correction to predict Stress Intensity Factors. The results give a good compromise to the theoretical one. The experimental result also gives significant data for the two dimensional mixed mode loading conditions.

Keywords: Stress intensity factors; Photoelasticity

1 INTRODUCTION

DURING recent years the fracture mechanics has obtained a special importance for predicting the material behavior under static and dynamic loading situation. Several catastrophic failures, over the years, have resulted in a sharp awareness of the effect of the cracks and stress raiser in the manufactured parts on their failure strength. The strength of a structure could be severely affected by the presence of crack like defects or pre-existing cracks and the defects are unavoidable in a cost effective manufacturing process. Since there are limitations on minimum size of the defects that can be detected, one needs to know the relation between the defect size and the strength of a structure. Fracture mechanics provides a methodology through which a quantitative relationship between the applied stress on a structure, defect size present, inherent properties of material and the fracture resistance characteristics of structure may be obtained. The stress intensity factor is generally used to characterize the crack tip stress field in the linear elastic situation. The stresses in the vicinity of a crack tip can be characterized by a single parameter called the Stress Intensity Factor (SIF). The SIF can be determined analytically only for relatively simple components and loadings. Most of the investigation established their approach by analytically generating isochromatic loops for plate type specimens containing a single edge crack. In all photo elastic methods more than one isochromatic fringe loop is required to extract the SIF, except for Irwin's two parameter approach, which suffers from the error normally associated with the measurements of angles and the difficulty in defining both the origin of the crack tip and the apogee of fringe. The effective methods of experimentally determining the stress intensity factor for a body containing a crack is to analyze the isochromatic pattern obtained from a photo elastic model.

Measurements of the fringe order N and position parameters r & θ, which locate one point or a number of points on a fringe loop are sufficient to permit the determination of K_I, K_{II} and σ_{ox}.. There are several methods which are limited to determine only two (i.e. K_I, and σ_{ox} or K_I and K_{II}) of the three quantities which affect the fringe pattern. Also most of the methods developed to employ isochromatic data from only one or two points in the fringe field which do not fully utilize the available data. Most of the studies for evaluating mixed mode stress intensity factor are

* Corresponding author.
E-mail address: vks2319@yahoo.co.in (V.K. Singh).

for uniaxial loading. Experimental study of the effect of biaxial load factor, specimen geometry on stress field parameters K_I, K_{II} and σ_{ox} is very limited. Whereas it is a well-known fact that these factors have a significant effect on the crack growth under mixed mode loading.

2 THEORY

The cracks in most of the structures of engineering importance may be located or developed during the service in the zones of stress concentration and the crack may be large enough so that the crack-tip may be closer to a boundary. The basic stress field equations of fracture mechanics are developed for cracks lying in a body of infinite dimensions (i.e. the crack-tips are far away from the boundaries) subjected to a uniform stress field. When only the first term (singular solution) of these equations are attempted to be applied for solving real life problems, one gets erroneous results. The recognition of this fact has led the researchers to account for this effect and multi parameter stress field equations have been developed in the last two decades. The role of photoelasticity in the development of multi parameter stress field equations are brought out in this context.

The stress optic law relates the fringe order N and principal stresses σ_1 and σ_2 as [1]

$$\frac{Nf_\sigma}{t} = \sigma_1 - \sigma_2 \tag{1}$$

For a plane stress problem the principal stresses are

$$\sigma_1,\ \sigma_2 = \frac{\sigma_x + \sigma_y}{2} \pm \sqrt{\left(\frac{\sigma_x + \sigma_y}{2}\right)^2 + (\sigma_{xy})^2} \tag{2}$$

For the purpose of mixed mode study, the stresses in the local neighborhood of a crack tip (r/a<1) can be approximated by Westergaard Stress component σ_{ij} in an increasing order power series as follows [2]

$$\begin{aligned}\sigma_x = \sigma_{ox} &+ \frac{K_1}{2\sqrt{\pi a}}\left\{\left(\frac{r}{2a}\right)^{-1/2}\cos\frac{\theta}{2}\left(1-\sin\frac{\theta}{2}\sin\frac{3\theta}{2}\right)+\frac{3}{2}\left(\frac{r}{2a}\right)^{1/2}\cos\frac{\theta}{2}\left(1+\sin^2\frac{\theta}{2}\right)\right.\\ &\left.+\sum_{n=1}^{\infty}\left(\frac{r}{2a}\right)^{n+1/2}C_n\left[\cos\left(n+\frac{1}{2}\right)\theta-\left(n+\frac{1}{2}\right)\sin\theta\sin\left(n-\frac{1}{2}\right)\theta\right]\right\}\\ &+\frac{K_{11}}{2\sqrt{\pi a}}\left\{-\left(\frac{r}{2a}\right)^{-1/2}\sin\frac{\theta}{2}\left(2+\cos\frac{\theta}{2}\cos\frac{3\theta}{2}\right)+\frac{3}{2}\left(\frac{r}{2a}\right)^{1/2}\sin\frac{\theta}{2}\left(2+\cos^2\frac{\theta}{2}\right)\right.\\ &\left.+\sum_{n=1}^{\infty}\left(\frac{r}{2a}\right)^{n+1/2}C_n\left[2\sin\left(n+\frac{1}{2}\right)\theta+\left(n+\frac{1}{2}\right)\sin\theta\cos\left(n-\frac{1}{2}\right)\theta\right]\right\}\end{aligned} \tag{3}$$

$$\begin{aligned}\sigma_y = &\frac{K_1}{2\sqrt{\pi a}}\left\{\left(\frac{r}{2a}\right)^{-1/2}\cos\frac{\theta}{2}\left(1+\sin\frac{\theta}{2}\sin\frac{3\theta}{2}\right)+\frac{3}{2}\left(\frac{r}{2a}\right)^{1/2}\cos^3\frac{\theta}{2}\right.\\ &\left.+\sum_{n=1}^{\infty}\left(\frac{r}{2a}\right)^{n+1/2}C_n\left[\cos\left(n+\frac{1}{2}\right)\theta+\left(n+\frac{1}{2}\right)\sin\theta\sin\left(n-\frac{1}{2}\right)\theta\right]\right\}\\ &+\frac{K_{11}}{2\sqrt{\pi a}}\left\{\left(\frac{r}{2a}\right)^{-1/2}\sin\frac{\theta}{2}\cos\frac{\theta}{2}\cos\frac{3\theta}{2}-\frac{3}{2}\left(\frac{r}{2a}\right)^{1/2}\sin\frac{\theta}{2}\cos^2\frac{\theta}{2}\right.\\ &\left.-\sum_{n=1}^{\infty}\left(\frac{r}{2a}\right)^{n+1/2}C_n\left(n+\frac{1}{2}\right)\sin\theta\cos\left(n-\frac{1}{2}\right)\theta\right\}\end{aligned} \tag{4}$$

$$\sigma_{xy} = \frac{K_1}{2\sqrt{\pi a}}\left\{\left(\frac{r}{2a}\right)^{-1/2}\sin\frac{\theta}{2}\cos\frac{\theta}{2}\cos\frac{3\theta}{2} - \frac{3}{2}\left(\frac{r}{2a}\right)^{1/2}\sin\frac{\theta}{2}\cos^2\frac{\theta}{2}\right.$$
$$\left. -\sum_{n=1}^{\infty}\left(\frac{r}{2a}\right)^{n+1/2} C_n\left(n+\frac{1}{2}\right)\sin\theta\cos\left(n-\frac{1}{2}\right)\theta\right\}$$
$$+\frac{K_{11}}{2\sqrt{\pi a}}\left\{\left(\frac{r}{2a}\right)^{-1/2}\cos\frac{\theta}{2}\left(1-\sin\frac{\theta}{2}\sin\frac{3\theta}{2}\right)+\frac{3}{2}\left(\frac{r}{2a}\right)^{1/2}\cos\frac{\theta}{2}\left(1+\sin^2\frac{\theta}{2}\right)\right. \quad (5)$$
$$\left.+\sum_{n=1}^{\infty}\left(\frac{r}{2a}\right)^{n+\frac{1}{2}} C_n\left[\cos\left(n+\frac{1}{2}\right)\theta-\left(n+\frac{1}{2}\right)\sin\theta\sin\left(n-\frac{1}{2}\right)\theta\right]\right\}$$

where $C_n = (-1)^n\left(\frac{2n+3}{2n+2}\right)\frac{1\times3\times.....\times(2n-1)}{2\times4\times.....2n}$; substituting Eqs. (2-5) into (1), we get

$$\left(\frac{N f \sigma}{t}\right)^2 = \frac{K_I}{2\sqrt{\pi a}}\left\{\left(\frac{r}{2a}\right)^{-1/2}\cos\frac{\theta}{2}\left(2\sin\frac{\theta}{2}\sin\frac{3\theta}{2}\right)+3\left(\frac{r}{2a}\right)^{1/2}\cos^3\frac{\theta}{2}-3\left(\frac{r}{2a}\right)^{1/2}\cos\frac{\theta}{2}+\sum_{n=1}^{\infty}\left(\frac{r}{2a}\right)^{n+\frac{1}{2}}C_n\left[2\left(n+\frac{1}{2}\right)\sin\theta\sin\left(n-\frac{1}{2}\right)\theta\right]\right\}$$
$$+\frac{K_{II}}{2\sqrt{\pi a}}\left\{\left(\frac{r}{2a}\right)^{-1/2}\left(2\sin\frac{\theta}{2}\cos\frac{\theta}{2}\cos\frac{3\theta}{2}\right)+\left(\frac{r}{2a}\right)^{-1/2}2\sin\frac{\theta}{2}-\frac{3}{2}\left(\frac{r}{2a}\right)^{\frac{1}{2}}2\sin\frac{\theta}{2}\cos^2\frac{\theta}{2}-\frac{3}{2}\left(\frac{r}{2a}\right)^{1/2}2\sin\frac{\theta}{2}\right.$$
$$\left.-\sum_{n=1}^{\infty}\left(\frac{r}{2a}\right)^{n+\frac{1}{2}}C_n\left[2\sin\left(n-\frac{1}{2}\right)\theta\right]-\sigma_{0x}\right\}^2+\frac{K_1}{2\sqrt{\pi a}}\left\{\left(\frac{r}{2a}\right)^{-1/2}\sin\frac{\theta}{2}\cos\frac{\theta}{2}\cos\frac{3\theta}{2}-\frac{3}{2}\left(\frac{r}{2a}\right)^{1/2}\sin\frac{\theta}{2}\cos^2\frac{\theta}{2}\right.$$
$$\left.-\sum_{n=1}^{\infty}\left(\frac{r}{2a}\right)^{n+1/2}C_n\left(n+\frac{1}{2}\right)\sin\theta\cos\left(n-\frac{1}{2}\right)\theta\right\}+\frac{K_{11}}{2\sqrt{\pi a}}\left\{\left(\frac{r}{2a}\right)^{-1/2}\cos\frac{\theta}{2}\left(1-\sin\frac{\theta}{2}\sin\frac{3\theta}{2}\right)\right.$$
$$\left.+\frac{3}{2}\left(\frac{r}{2a}\right)^{1/2}\cos\frac{\theta}{2}\left(1+\sin^2\frac{\theta}{2}\right)+\sum_{n=1}^{\infty}\left(\frac{r}{2a}\right)^{n+\frac{1}{2}}C_n\left[\cos\left(n+\frac{1}{2}\right)\theta-\left(n+\frac{1}{2}\right)\sin\theta\sin\left(n-\frac{1}{2}\right)\theta\right]\right\} \quad (6)$$

The *N-K* relation given in Eq. (6) is non-linear in terms of the three unknowns K_I, K_{II} and σ_{ox}. In the present analysis, three points deterministic approach have been used. In this approach, data is selected from three arbitrary points (r_1, θ_1), (r_2, θ_2) and (r_3, θ_3). The Newton-Raphson [3] method is applied to solve the three simultaneous non-linear equations. The convergence of this method is rapid and three or four iterations are sufficient for obtaining precise results for K_I, K_{II} and σ_{ox}. Fig. 1 shows that in Sih equation, five terms are sufficient for the stress calculation ahead of the crack tip. More than five numbers of terms have the same effect; hence five numbers of terms are used for calculation of stress field parameters.

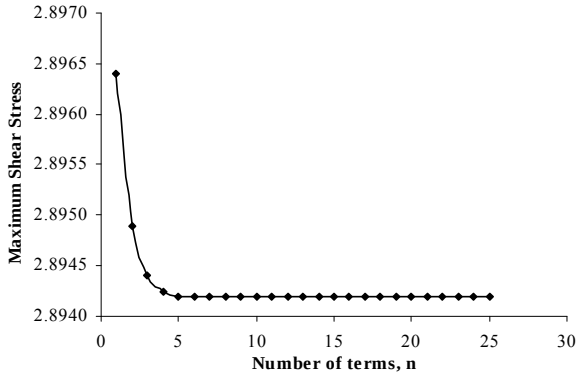

Fig. 1
Effect of number of terms on stress field.

3 MATERIAL AND METHOD

The stress distribution in the stressed model can be analyzed by using the photo-elasticity method. It occupies prominent place because the method is cheaper, faster and more accurate than any other experimental procedure. The method is proposed for determining the modulus of elasticity, material fringe value etc. To study or to evaluate the mixed mode SIF, photoelastic method specimen were prepared from the cast material Araldite CY-230 (100 part by weight) and Hardener HY-951(9 part by weight).The square piece of $100\times100\times2$ mm^3 size were cut from cast plate. Mechanical slits were made at the centre of the plate at required angle of inclination with respect to vertical loading axis by drilling a hole of diameter (2 mm) and then cutting by jewelry saw to simulate the natural crack. The ends of mechanical sheet were further extended by razor blades by an amount 0.2 to 0.5 mm. The final lengths were kept 12, 16 and 20 mm and crack inclination angle were taken 0^0, 30^0, 45^0 and 60^0. The crack tip radius/ crack length were taken less than 0.02 mm. The above results approached very near the investigation of Etheridge and Dally [4]. Photo elastic properties are obtained by Tardy's compensation method [1].

As the reaction of resin and hardener is exothermic, a large amount of heat is librated, because of which when the percentage of hardener in the resin is increased; the curing time is also increased. Prolong curing time or increasing the curing temperature gives slightly better thermal stability and thus constant mechanical and electrical properties over a large range of temperature [5]. For finding out the proportionality limits and modulus of elasticity beam strips of different width and thickness, equal to the thickness of casted sheet were cut from the sheet with the help of slitting cutter on the milling machine. The specimen (Fig. 2) was loaded on Instron Universal Testing Machine, model 6051 of 5 kN capacity with a crosshead speed 0.1 mm/min. The programme for tensile test was loaded in the console control to obtain the proportionality limits and modulus of elasticity.

For finding out the material fringe value a circular disc (Fig. 3) diameter 60 mm was made from the casted sheet by turning on the model making lathe. The circular disc was loaded diametrically at different loads for the observations at the centre of the disc. For this instance, the equation of material fringe value becomes [1]

$$f_\sigma = \frac{8p}{\pi DN} \tag{7}$$

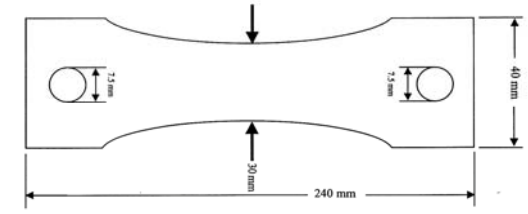

Fig. 2
Specimen geometry for tensile test.

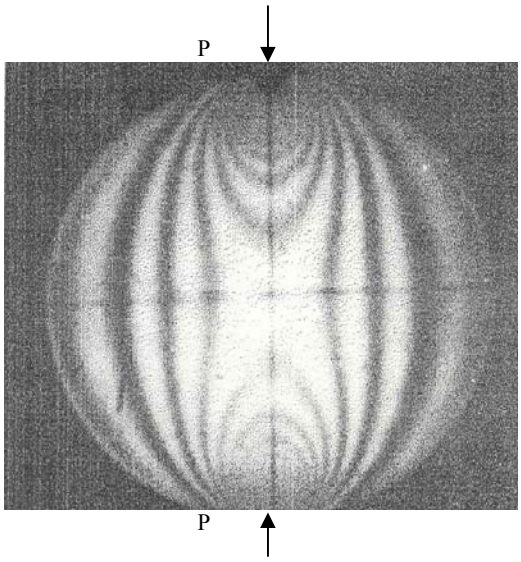

Fig. 3
Specimen geometry and loading condition for diametral compression.

or

$$f_\sigma = \frac{8}{\pi D} \text{ (slope of the curve drawn between } p \text{ vs. } N) \tag{8}$$

It was noted that the value of f_σ is independent of model thickness '*h*'. For the stress analysis by photoelastic method, object is simulated by photo elastic model. Photo elastic material which has low fringe value, high value of figure of merit, high value of sensitivity index , high value of modulus of elasticity and high value of proportional limits is preferred for making of photoelastic model, which is justified as discussed below. Eq. (1) can be written as

$$\frac{Nf_\sigma}{2t} = \tau_{\max} \tag{9}$$

Above equation shows that for constant shear stress ($\tau_{\max}$), *N* will be large if f_σ is small. For higher optical sensitivity, index material should have a lower material fringe values (f_σ). For this reason, low fringe value is preferred. The deformation of photoelastic material should be as small as possible for stress analysis (deformation should be within the elastic limit). For this reason, large Modulus of elasticity and large proportional limits are preferred [10]. Fig. 4 shows that material fringe value is minimum, when 8% (by weight) hardener (HY-951) is mixed with resin (CY-230) and all other material properties tend to increase. Fig. 4 shows that as a compromise between material fringe value and modulus of elasticity 8% to 9% of hardener is best for conducting the experiments on the resin (CY-230) with hardener (HY- 951) as per the requirement of photoelastician. For the present investigation, 9% was used.

3.1 Data collection and measurement using CAD software

Currently, direct eye observation method is being adopted for determining fringe order at the point of interest for stress analysis to minimize the error due to direct observation of fringe order at the point of interest. For this purpose, photographs from the screen under different loading were taken. Photographs taken from the experimental setup were scanned. The scanned photographs were loaded in CAD software for the measurement of fringe order at the different points from the crack-tip. Fig. 5 shows three points on the fringe pattern *A*, *B* & *C*, respectively. OP distance shows the half crack length '*a*'. To verify the accuracy of the present method the same point locations *A*, *B* & *C* are selected and were marked by a marker on the experimental model and ten photographs were taken for the same loading condition. These photographs were taken by different person and at different time span. All ten photographs were used for the measurement of position of interest point i.e. *r* and θ values. All measured values of *r* and θ for same loading are shown in Table 1.

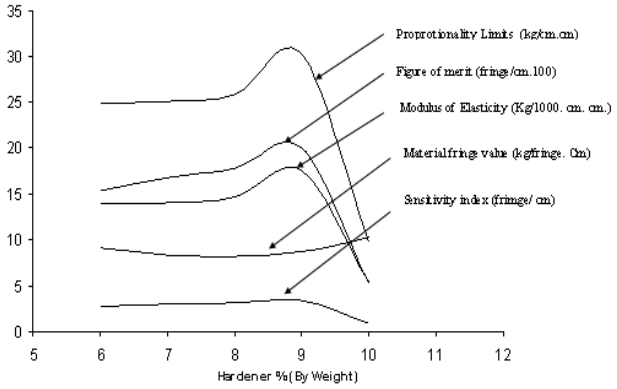

Fig. 4
Material properties of CY-230 with different percentage of Hardener (HY-951).

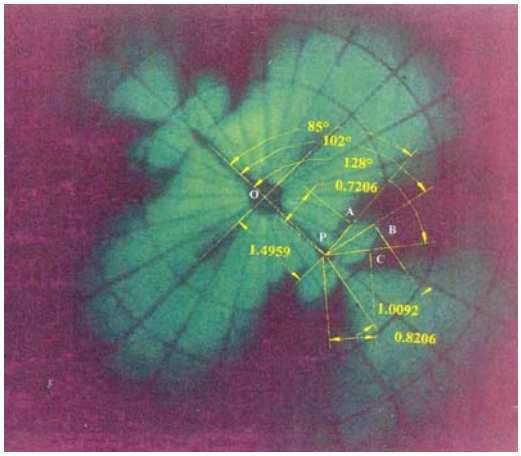

Fig. 5
Image processing and measurement of fringe position from crack tip using CAD software.

Table 1
Measured r and θ using CAD-software and the statistical properties

S. No	$r1$ (mm)	θ_1 (degree)	r2 (mm)	θ_2 (degree)	r3 (mm)	θ_3 (degree)
1.	4.817	95	6.746	78	5.488	52
2.	4.702	95	6.750	78	5.473	52
3.	4.817	95	6.740	78	5.460	52
4.	4.817	95	6.732	78	5.455	52
5.	4.820	95	6.749	78	5.485	52
6.	4.820	95	6.752	78	5.485	52
7.	4.808	95	6.733	78	5.483	52
8.	4.812	95	6.745	78	5.491	52
9.	4.821	95	6.731	78	5.485	52
10.	4.817	95	6.731	78	5.485	52
Mean	4.805	95	6.740	78	5.477	52
Std. Deviation	0.0345	0	0.025	0	0.0349	0
Co-efficient of variance	0.0071	0	00037	0	0.0063	0

4 RESULT AND DISCUSSION

4.1 Stress intensity factor K_I

The effect of biaxial load factor k on stress intensity factor (K_I) is shown in Fig. 6(a) for a/W=0.06 and different crack angles. Fig. 6(a) shows that K_I increases as k increases. This may be due to increase in plastic zone size produced ahead of the crack-tip. It is well known that in a stressed body or plate, the stress exceeds the yield strength near the crack tip and a plastic zone develops. The actual shape and size of the plastic zone depends on the plastic flow of the material and it is proportional to $(K_I/\sigma_o)^2$. Due to this, as k increases the position and size of the plastic zone ahead of crack line increases. The position and extent of minimum value of plastic zone size is also highly influenced by biaxial load factor. Similar results are also found in the work of Du and Hancou [6] and Poul [7]. As the plastic zone size is proportional to square of stress intensity factor K_I, it can be said that for a given crack position, K_I should increase when k is increased. Hence, the experimental results which have been depicted here show increasing behavior with k. The effect of crack angle on the (K_I) is shown in Fig. 6(b) for different k values. Fig. 6(b) shows that K_I decreases when $\alpha < 45°$ and there after it increases for all k values. At the crack angle α = 45° maximum change in K_I occurs. This may be due to the change of crack position from minimum loading direction (σ-axis) to maximum loading direction ($k\sigma$-axis). The experimental result shows that over all values of K_I decreases with increasing crack angle. The theoretical relation available for K_I is written as

$$K_I = \frac{\sigma\sqrt{\pi a}}{2}\left[(1+k)+(1-k)\cos 2\theta\right] \tag{10}$$

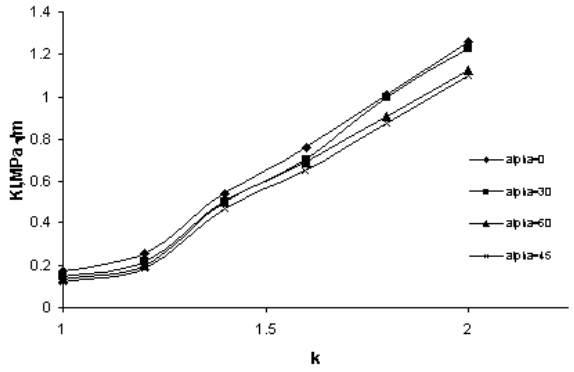

Fig. 6(a)
Effect of biaxial factor on stress intensity factor K_I for $a/W = 0.06$.

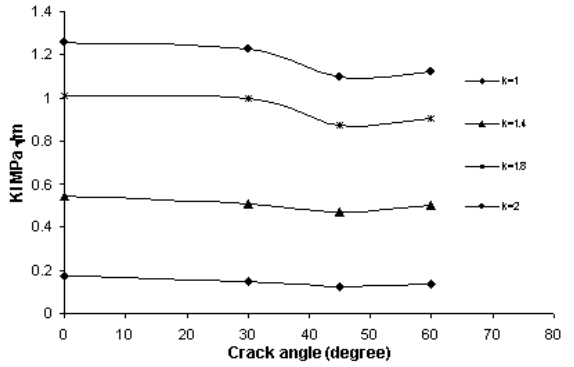

Fig. 6(b)
Effect of crack angle on stress intensity factor K_I for a/W = 0.06.

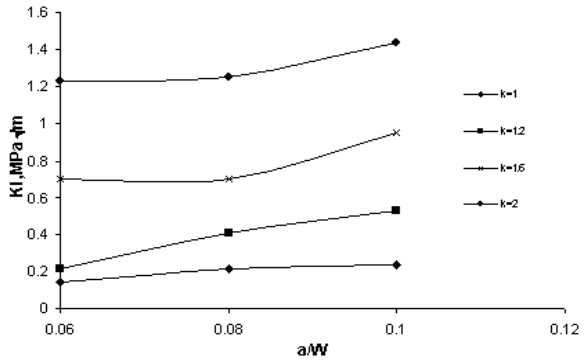

Fig. 6(c)
Effect of (a/W) ratio on stress intensity factor K_I for $\alpha = 30°$.

This relation is based on assumption of infinite plate with remote loading conditions for all α values. For $\alpha = \pi/2$, Eq. (10) will reduce to

$$K_I = \sigma\sqrt{\pi a} \tag{11}$$

and $\alpha = \pi/4$, Eq. (10) becomes

$$K_I = \frac{\sigma\sqrt{\pi a}}{2}(1+k) \tag{12}$$

Eqs. (8) and (9) show that K_I is independent of crack angle α. The bracketed term in Eq. (10) will be positive for $k>1$ but more significant when $\alpha \leq 45°$. In case of $k = 1$ the maximum load is equal to minimum load. In this case K_I is independent of crack angle α. Theoretical result also shows that for $k = 1$, K_I is constant for all value of α. The

experimental value also shows this type of trend in Fig. 6(b) for k =1 and the value of K_I is approximately constant. Lee, Liebowitz and Eftis [8] have proposed analytically and numerically that stress intensity factor, depends on the (L/a) and (W/a), where L is the length of specimen and W is the width of the specimen. For horizontal crack, Hafelle and Lee [9] have also studied the effect of specimen geometry factor ($2a/W$) and ($2L/W$) under pure Mode I loading. The dependence of K_I on (a/W) is shown in Fig. 6(c) for different crack angle and biaxial load factor. Fig. 6(c) shows that K_I increases when a/W increases form 0.06 to 0.1. The theoretical relation also gives similar trend. In the present investigation, it is seen that K_I depends upon crack angle, biaxial load factor, constant stress term and geometry factor (a/W) and (a/L). Hence, an attempt has been made to correlate these parameter to K_I and following from is presented

$$K_I = \sigma\sqrt{\pi a}\left[(1+k)+(1-k)\cos 2\theta\right] f_1\left(\frac{L_e}{W_e}\right) \tag{13}$$

where $L_e = L/2 - a.\cos\alpha$ and $W_e = W/2 - a.\sin\alpha$, (given in Fig. 7). The function f_1 (L_e/W_e) is obtained from regression analysis and found as

$$f_1\left(\frac{L_e}{W_e}\right) = \left[a_1 + a_2\left(\frac{L_e}{W_e}\right) + a_3\left(\frac{L_e}{W_e}\right)^2 + a_4\left(\frac{L_e}{W_e}\right)^3 + a_5\left(\frac{L_e}{W_e}\right)^4\right] \tag{14}$$

The coefficient (a_1 to a_5) are shown in Table 2 for various biaxial factor.

4.2 Stress intensity factor K_{II}

The variation of K_{II} with biaxial factor k is shown in Fig. 8(a) indicates that K_{II} decreases as k increases for a given crack angle. The variation of K_{II} with k is found to be similar to the theoretical variations. Fig. 8(b) shows the effect of crack angle α on K_{II}.

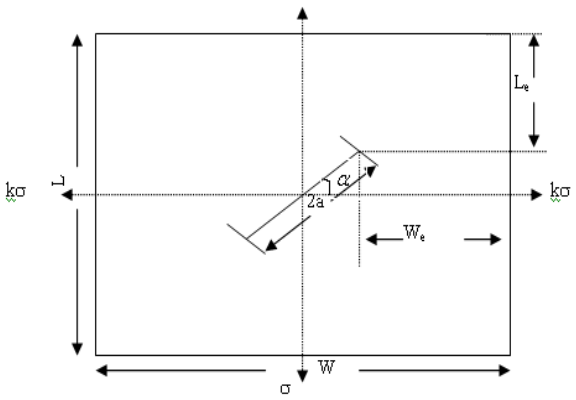

Fig. 7
Effective length and effective width in the specimen.

Table 2
The coefficient of Eq. (14)

k	Coefficients				
	a_1	a_2	a_3	a_4	a_5
1.0	2958.13	-12319.36	19224.87	-13324.242	3460.51
1.2	4537.08	18372.43	27972.43	-18972.07	4837.87
1.4	15558.09	-64654.20	100712.02	-69686.75	18072.87
1.6	25511.84	-105574.57	163730.04	-112775.23	29110.39
1.8	13629.04	-56212.08	87054.91	-59991.82	15522.33
2.0	42527.06	-175971.91	272858.97	-187899.41	48486.72

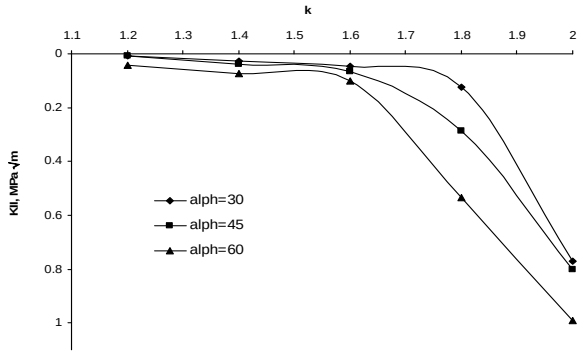

Fig. 8(a)
Effect of biaxial factor on stress intensity factor *K*II for $a/W = 0.08$.

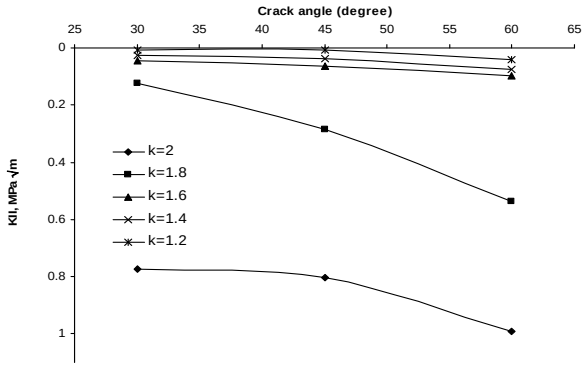

Fig. 8(b)
Effect of crack angle on stress intensity factor K_{II} for $a/W = 0.06$.

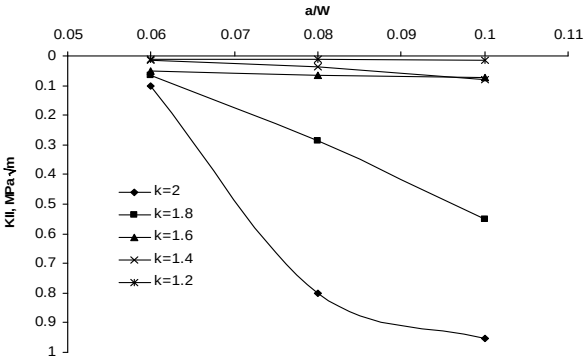

Fig. 8(c)
Effect of a/W on stress intensity factor K_{II} for $\alpha = 45°$.

Slight decrease in K_{II} with α is seen in Fig. 8(b) in some cases of biaxial load factor. This type of behavior is seen mostly for higher biaxial factor ($k > 1.6$). The magnitude of K_{II} is found to be constant or slightly increase and then decrease when $k < 1.6$. The theoretical values decrease up to $\alpha < 45°$ then increases with increase in α for all value of k. Fig. 8(c) shows the effect of (a/W) on K_{II} for different crack angles and biaxial factor. It is seen that K_{II} becomes constant for $\alpha = 45°$ beyond $a/W = 0.08$ values. In Fig. 8, K_{II} is higher for higher value of k. Fig. 8(c) shows that the value of K_{II} is of the order of 10^{-8} to 10^{-7} for all cases of (a/W) for $k = 1$. The theoretical value of K_{II} for $k = 1$ is zero. It reveals for the Fig. 8(a-c) that K_{II} depends on α, k and a/w. The magnitude obtained from experiments is also quite different from the theoretical solutions for same boundary conditions and loading. This is due to the geometry constraint. Hence, a geometry factor is derived for K_{II} and presented in following form

$$K_{II} = \frac{\sigma\sqrt{\pi a}}{2} f_2\left(\frac{L_e}{W_e}\right) \tag{15}$$

Table 3
Coefficient of Eq. (16)

k	Coefficients				
	a_{21}	a_{22}	a_{23}	a_{24}	a_{25}
1.0	0.023338	-0.006552	0.0149691	-0.103077	0.026600
1.2	166886.0	-484369.54	751914.84	-518243.74	133810.83
1.4	52169.22	-215980.16	334828.70	-230670.93	59558.42
1.6	5040.72	-22239.70	36592.78	-26637.27	7234.41
1.8	8273.014	-34264.72	53203.89	-36704.137	9492.012
2.0	2974206.0	-12400926.0	19376463.0	-13446820.0	3497075.3

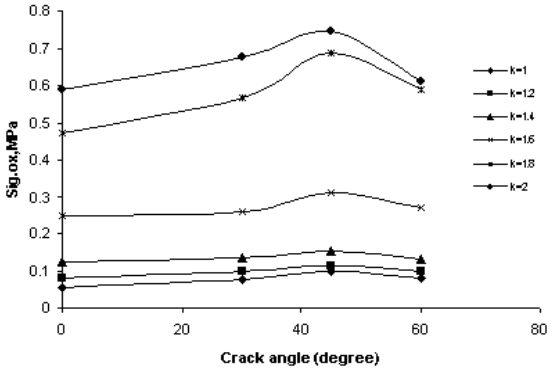

Fig. 9(a)
Effect of crack angle on Sig.ox, for $a/W = 0.06$.

where the function f_2 (L_e/W_e) is obtained from regression analysis and found as

$$f_2\left(\frac{L_e}{W_e}\right)=\left[a_{21}+a_{22}\left(\frac{L_e}{W_e}\right)+a_{23}\left(\frac{L_e}{W_e}\right)^2+a_{24}\left(\frac{L_e}{W_e}\right)^3+a_{25}\left(\frac{L_e}{W_e}\right)^4\right] \tag{16}$$

The coefficient (a_{21} to a_{25}) are shown in Table 3 for various biaxial factor.

4.3 Constant stress term, σ_{ox}

The effect of biaxial load factor, crack angle and specimen geometry parameter a/W and a/L are shown in Fig. 9(a-b). Fig. 9(a) shows that σ_{ox} increases as α increases upto $\alpha < 45°$ for all a/W ratios. There after, it shows decreasing tendency. When $\alpha < 45°$, the crack is towards the minimum loading axis. In this case the net area in the length direction of the specimen becomes more significant than net area in the width direction of the specimen as in our analysis, biaxial load factor $k \geq 1$. The net effective dimension in length direction and width direction are defined in Fig. 7.

L_e (effective length)$=L/2 - a \cos \alpha$.
W_e (effective width)$=W/2 - a \sin \alpha$.

Now as α increases from $\alpha = 0$ to $\alpha < 45°$, L_e increases and W_e decreases. In this case, (α<45°) L_e is more significant than W_e and as L_e/W_e increases Sig.ox (σ_{ox}) shows increasing tendency whereas when α exceeds 45°, W_e becomes more significant than L_e. For $\alpha > 45°$, Le_e/W_e shows decreasing tendency as α is increased from $\alpha = 45°$ to higher value and hence σ_{ox} shows decreasing tendency. Hence, it can be said that sig,ox (σ_{ox}) depends upon the width factor (W/a) and length factor (L/a) or combining we can say geometry factor (L_e/W_e). Lee, Liebowitz and Eftis [7] have also proved for horizontal crack that the constant stress term as denoted by 'A' should be the fraction of (L/a) and (W/a) and suggested a geometry correcting factor containing non-dimensional parameter (W/a) and (L/a) for sig.ox (σ_{ox}). The effect of biaxial load factor on sig.ox is shown in Fig. 9(b). An increasing tendency with k

is seen in Fig. 7 (b) for all crack angles and biaxial load factor. Fig. 9(b) also shows that when k exceeds 1.6 the difference in σ_{ox} values for a given crack angle is more as compared to $k < 1.6$. This type of behavior is seen for all a/W ratios taken in the present investigation. Similar differences are also seen for K_I. The effect of a/W on σ_{ox} is shown in Fig. 9(c) for $\alpha = 30$ and different biaxial factor k. From the present analysis, it can be said that σ_{ox} depends on geometry parameters (a/L) and (a/W) and biaxial factor k. Hence an attempt has been made to correlate these parameter with the experimentally obtained σ_{ox} value. From the present experimental results, it is proposed that σ_{ox} may be written in form of

$$\sigma_{ox} = -\left[f_3\left(\frac{L_e}{W_e}\right) - k \right]\sigma \tag{17}$$

Where σ= is the applied stress; k= biaxial factor and $f_3\left(\frac{L_e}{W_e}\right)$ = geometry factor.

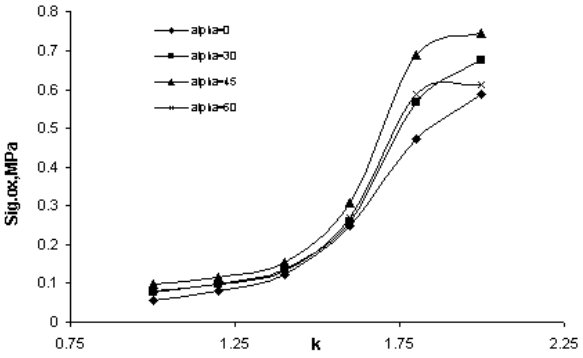

Fig. 9(b)
Effect of biaxial factor on Sig.ox, for $a/W = 0.06$.

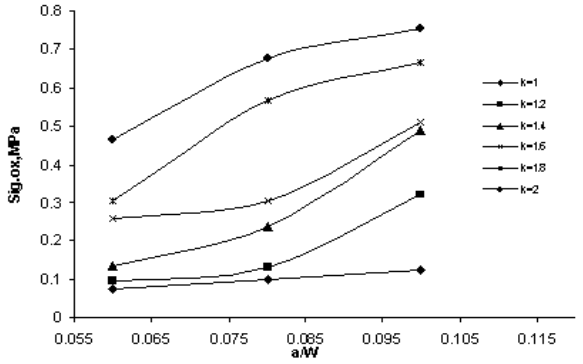

Fig. 9(c)
Effect of (a/W) on Sig.ox, for $\alpha = 30°$.

Table 4
Coefficient of Eq. (18)

k	Coefficients				
	a_{31}	a_{32}	a_{33}	a_{34}	a_{35}
1.0	-702.15	2995.24	-4774.03	3374.71	-892.68
1.2	6484.74	-26616.45	40951.69	-27988.54	7169.68
1.4	14510.60	-59920.26	92735.20	-63745.92	16421.54
1.6	10367.84	-42619.08	65658.29	-44924.94	11519.13
1.8	8356.27	-34106.06	52145.22	-35390.82	8996.79
2.0	8573.45	-34850.31	53065.16	-35866.77	9079.93

Table 5
τ_{max}/τ'_{max}, value

S. No.	k	τ_{max}/τ'_{max},			
		$\alpha = 0°$	$\alpha = 30°$	$\alpha = 45°$	$\alpha = 60°$
1.	1.0	0.8849	0.69225	0.59215	0.63388
2.	1.2	0.98657	0.87685	0.8386	0.95862

The function f_3 is obtained from the regression analysis technique and expressed as

$$f_3\left(\frac{L_e}{W_e}\right) = \left[a_{31} + a_{32}\left(\frac{L_e}{W_e}\right) + a_{33}\left(\frac{L_e}{W_e}\right)^2 + a_{34}\left(\frac{L_e}{W_e}\right)^3 + a_{35}\left(\frac{L_e}{W_e}\right)^4\right] \tag{18}$$

The coefficients (a_{31} to a_{35}) are shown in Table 4 for various biaxial factor.

4.4 Comparative studies

To compare the experimental results with theoretical values, Table 5 presents the ratio of τ_{max}/τ'_{max}, where τ_{max} is obtained from two-term theoretical solution. Table 5 shows that values are very near to unity, but not exactly one. This difference may be due to non-inclusion of higher order stress terms in the theoretical prediction for σ=32.48 kg/mm^2, a= 10 mm and k= 1. The comparative results show a good agreement between experimental and theoretical results.

REFERENCES

[1] Singh S., 1983, *Applied Stress Analysis*, Khanna Publishers, Delhi, India, 346-363.
[2] Sih G.C., 1973, A special theory of crack propagation methods of analysis and solution of crack problems, *Journal of Mechanics of Fracture* **1**: XXI-XLV.
[3] Kelley L.G., 1991, *Handbook of Numerical Method and Applications*, Addison-Werly, Reading Mass, p. 99.
[4] Etheridge, J.M., Dally, J.W., 1977, A critical review of methods for determining stress-intensity factors from isochromatic fringes, *Journal of Experimental Analysis* **17**: 248-254.
[5] Irwin G.R., 1957, Analysis of stress and strains near the end of a crack traversing a plate, *ASME Transactions, Journal of Applied Mechanics* **24**(3).
[6] Du Z.Z., Hancock J.W, 1991, The effect of non singular stress on crack tip constant, *Journal of Mechanics and Physics of Solids* **39**: 555-569.
[7] Paul T.K., 1995, Plane stress mixed mode fatigue crack propagation, *Engineering Fracture Mechanics* **52**.
[8] Liebowitz H., Lee J.D., Eftis J., 1978, Biaxial load effects in fracture mechanics, *Engineering Fracture Mechanics* **10**: 315-335.
[9] Haefele P.N., James D. Lee, 1995, The constant stress term, *Engineering Fracture Mechanics* **50**(5/6): 869-882.
[10] Singh V.K., M. Tech Thesis, 2002, Experimental investigation of mixed mode stress field parameters under biaxial loading condition, G.B. Pant University of Ag & Technology, Pantnagar.